# Nanorod orientation control by swift heavy ion irradiation

Korkos, Spyridon

2022-04-25

Korkos , S , Jantunen , V , Arstila , K , Sajavaara , T , Leino , A , Nordlund , K & Djurabekova , F 2022 , ' Nanorod orientation control by swift heavy ion irradiation ' , Applied Physics Letters , vol. 120 , no. 17 , 171602 . https://doi.org/10.1063/5.0089028

http://hdl.handle.net/10138/347979
https://doi.org/10.1063/5.0089028

unspecified
acceptedVersion

# Nanorod orientation control by swift heavy ion irradiation

Spyridon Korkos[1,2], Ville Jantunen[3], Kai Arstila[1,2], Timo Sajavaara[1,2], Aleksi Leino[3], Kai Nordlund[3], Flyura Djurabekova[3]
[1] *Accelerator Laboratory, Department of Physics, University of Jyvaskyla, P.O. Box 35, FI-40014 Jyvaskyla, Finland*
[2] *Nanoscience Center, Department of Physics, University of Jyvaskyla, P.O. Box 35, FI-40014 Jyvaskyla, Finland and*
[3] *Department of Physics, University of Helsinki, P.O. Box 43, FI-00014 Helsinki, Finland*

Highly energetic ions have been previously used to modify the shape of metal nanoparticles embedded in an insulating matrix. In this work, we demonstrate that energetic ions can be used not only for the shape modification, but also for manipulation of nanorod orientation. This observation is made by imaging the same nanorod before and after swift heavy ion irradiation using transmission electron microscope. Atomistic simulations reveal a complex mechanism of nanorod re-orientation: by an incremental change of its shape from a rod to a spheroid and further back into a rod aligned with the beam.

Shape modification of metallic nanoparticles (NPs) has been studied for a long time as a tool for tuning the optical properties of nanocomposite materials. Spherical Au NPs have distinctive absorbtion peaks at visible light, which changes with size [1]. When the shape of the NPs is made cylindrical, there are two absorbtion peaks corresponding to transversal and longitudal modes of the surface plasmons [1]. This means that the ability to control the shapes of NPs, allows for fine-tuning their response to light making them ideal candidates for future nanoscale optical devices. Embedding the metal nanoparticles inside certain insulator materials, such as silica, allows keeping them protected from the environment and conserving whatever shape modifications have been achieved, including the orientation of the rods. While it may be difficult to access the NPs embedded inside the surrounding material with other methods, it is known that they can be modified using swift heavy ion (SHI) irradiation (i.e. using ions with energies $E \sim 1$ MeV / amu). [2–16]

Shape transformation of spherical metal NPs into nanorods aligned in the beam direction was initially reported by d'Orléans *et al.* [17] and confirmed in multiple studies later [3, 5–8, 10–16]. Several explanations, such as the overpressure model by d'Orléans *et al.* [18] and the ion hammering effect by Roorda *et al.* [19] were suggested to explain the phenomenon. Although ion hammering effect is expected to modify any size of NPs, the SHI irradiation of NPs smaller than the track diameter did not cause the elongation effect [12]. On the other hand, the overpressure model was supported by molecular dynamics simulations [3] that gave an atomistic insight on expansion of molten nanoparticle into a softened and underdense track in silica.

Most studies on SHI irradiated NPs have focused on spherical NPs, while other shapes have received less attention. In this study we focus on gold nanorods inside a silica matrix and how they react to SHI irradiation. We chose a 45° angle of incidence, however, this choice is arbitrary and does not affect the observed result. We use TEM window grids as substrates to keep track of individual nanorods before and after the irradiation. To understand the shape modification mechanism, we use a multiscale molecular dynamics simulation model based on two-temperature approach [3, 5, 20–23] to gain further insight into the details of this process. Our experiments and simulations consistently show that swift heavy ion irradiation can be used to orient nanorods into the beam direction even when they remain fully inside the insulating matrix. This opens up a new way for flexible manipulation of nanorod orientation without a risk of chemical contamination.

*Experimental methods.* A 50 nm thick $SiO_2$ film was grown using plasma-enhanced chemical vapor deposition (PECVD) at 200 °C (Plasmalab80Plus by Oxford Instruments, $SiH_4$ and $N_2O$ as precursors) on top of a TEM grid with 20 nm thick $Si_3N_4$ windows. Chemically synthesized Au nanorods (Sigma-Aldrich, diameter 20–45 nm and length 30–90 nm) were dispersed on top of the film by dropcasting. The nanorods were then embedded by means of an additional 50 nm PECVD-$SiO_2$ film. The total layer thickness of 120 nm fulfills the requirements of the TEM imaging. Time-of-Flight Elastic Recoil Detection Analysis (ToF-ERDA) with 1.7 MV Pelletron accelerator and 11.9 MeV $^{63}Cu^{6+}$ beam [24] was used to measure the elemental composition of the deposited films at the Accelerator Laboratory of University of Jyväskylä.

The samples were irradiated by the 50 MeV $^{127}I^{9+}$ ion beam at 45° incidence in the TAMIA 5 MV tandem accelerator at Helsinki Accelerator Laboratory (University of Helsinki). The irradiation was performed to the fluence of $10^{14}$ ions/cm$^2$ at room temperature. The imaging of the irradiated samples was performed with a JEOL-JEM 1400 transmission electron microscope (TEM) operated at 120 kV. The direction of electron beam was chosen perpendicular to the ion beam direction used in the irradiation experiments. All the steps of this procedure are shown in figure 1.

*Simulation methods* To understand the rotation during irradiation, we used the classical molecular dynamics code PARCAS [25], which was used earlier for elongation simulaions of spherical nanoparticles [3, 16]. We gener-

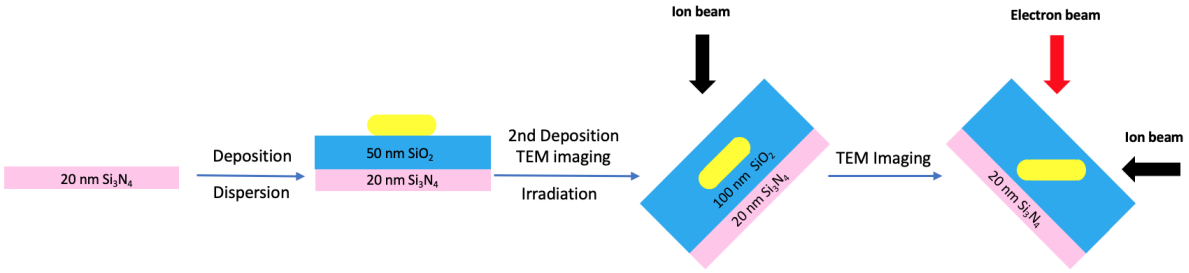


FIG. 1. Schematic representation of the experimental procedure. The sample during the second TEM stage (after irradiation) is placed in such a way that the TEM electron beam is directed perpendicular to the direction of the ion beam used during irradiation. This way the the dimensions of the actual nanorod were imaged instead of its projection.

ated a rectangular box of Au fcc lattice and cut out of it a nanorod of the required size. Since the size of the experimental nanorods is too large for efficient MD simulations, we reduced the size of the nanorods to 18 nm in length and 10 nm in width, while keeping the same aspect ratio as in the experimental ones. The nanorods were embedded inside the amorphous $SiO_2$ matrix similarly to Djurabekova and Nordlund [26]. In brief, the nanorod is first compressed by 2%, a cavity in silica is created with the shape and size of the original NP, and the NP is then fit inside the cavity so that it will expand to the empty space when it relaxes. The nanorods were initially aligned perpendicular to the ion beam direction.

Since the shape modification occurs only after high ion irradiation fluence, we adopted a similar approach to simulate the SHI effects in MD as described in Leino *et al.* [3]. We used the instant energy deposition profiles that were pre-calculated using the two-temperature *i*-TS model [27]. We used energy depositon profiles corresponding to both 50 MeV I and 164 MeV Au. We used the latter since it gave more efficient dynamics shape modification at higher irradiation energy, and hence was it was computationally more feasible to reach high fluences with the higher energy. Moreover, the melting point of the simulated silica is much higher compared to the experimentally observed values (3500K versus 1995K in experiments). To compensate for this difference we scaled the profile of the deposited energy in silica with the ratio of the melting points. The Au atoms were given a constant deposited energy of 0.5 eV/atom [3]. This energy was sufficient to melt the nanorod completely. The interatomic potentials were Watanabe-Samela [28, 29] for interactions in silica, EAM-like for Au-Au interactions [30, 31] and Ziegler-Biersack-Littmark (ZBL) [32] for Au-O and Au-Si interactions.

The system relaxation was done for 50 ps at pressure and temperature control [33] towards zero pressure and 300 K temperature. After the system was relaxed, radial energy deposition was added perpendicular to the major axis of the initial nanorod at random locations. The ion impact was then simulated for 100 ps in NVE. Berendsen temperature control [33] at 300 K was used within the thin boundary regions perpendicular to the ion direction to dampen oscillations from pressure waves and to emulate cooling provided by the bulk material in the experimental samples.

We note that the 100 ps simulation time, which we used for computational efficiency of MD simulations, was not enough to reach full recrystallization of the nanorods after the impacts. However, recrystallization is a critical step in the shape modification process as reported by Leino *et al.* [2], because the volume of the amorphized Au NP is too large to trigger the continuous material flow into opening ion tracks in subsequent simulations. The NP must shrink to nearly original volume (and density) during the cooldown stage for sufficient thermal expansion during the subsequent impact. Although we used a similar method as Leino *et al.* [2] and Amekura *et al.* [16] to account for recrystallization, we verified this method by running an independent one-nanosecond long MD simulation of relaxation of a modified NP, which showed that the modified shape of the NP did not change even after much slow cooling (see Section B in the Supplementary Material).

*Results.* In the analysis of the samples, the same nanoparticle was imaged before and after the irradiation, as shown in figure 2, where the subfigures (a) and (b) show the same area of the sample before and after the irradiation, respectively, with identical magnification. Moreover, the image shows that most nanorods are far from the others, which excludes possible interactions between them.

Since the ion beam induced shape modification of nanoparticles is sensitive to the matrix material properties [34], at first we performed the elemental composition analysis of the grown films using ToF-ERDA measurements. The analysis confirmed the close-to-stoichiometric elemental ratio of the as-grown silicon dioxide (2.04±0.02) and extensive presence of hydrogen (>7 at.%), which is known to be released from the $SiO_2$ thin film during a SHI impact [35]. The depth profiles and detailed description of the ToF-ERDA analysis can

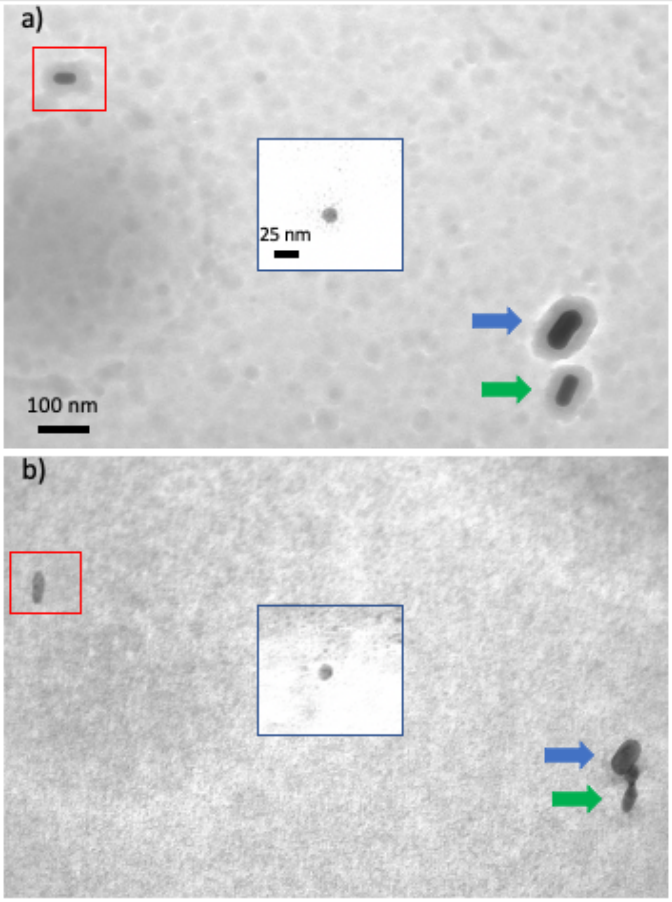


FIG. 2. TEM images of 20 nm $Si_3N_4$/50 nm $SiO_2$/NRs/50 nm $SiO_2$ sample imaged (a) before and (b) after irradiation with $^{127}I$ at $10^{14}$ ions/cm$^2$. The images were taken (a) from the top and (b) perpendicular to the ion beam direction.(The red box outlines the nanorod which "rotates"). The inset images in blue outline show a spherical nanoparticle (11.5 nm diameter) whose orientation did not change.

be found in the Section A of the Supplementary Material.

The analysis of a series of TEM images (totally 19) reveals that the nanorods within the diameter and length range from 20 to 31 nm and 32 to 63 nm, respectively, have changed their orientation, rotating to align with the ion beam direction after the fluence of $10^{14}$ ions/cm$^2$ (see figure 3). This is a curious observation, since the nanorods were embedded in a homogeneous matrix, which remained intact throughout the experiment. Furthermore, the length along the major axes of the rotated nanorods has still visibly increased. We also note that the nanorods outside of the indicated size range have not been seen to change their orientation (compare a large nanorod indicated by a blue arrow in figures 2a and b), although the size has somewhat shrunk due to significant ion fluence. The behavior of a second large nanorod (green arrow), which is still beyond the above-mentioned range, is less clear. It is apparent that this nanorod was initially shrinking and only after its size reached the range of sizes that are seen to rotate, its rotation begun. As shown in figure 2b, the angle between the nanorods indicated by the blue and green arrows increased. The rotation, however, has not been completed, as the ion fluence received by this nanorod after its size was reduced was lower. We do not observe substantial changes in the nanorods and spherical nanoparticles that are below 15 nm in width, see the inset images of figure 2. It is apparent that the irradiation at such high ion fluences causes disintegration of the small nanoparticles and subsequent re-assembling within the track. This results is consistent with previous work on nanospheres, which also were not found to change shape below a certain critical size [3, 13].

Furthermore, the TEM images of figure 3 reveal the polycrystallinity of the nanorods after the irradiation. Rizza *et al.* [36] suggested that the presence of grains implies that the phase transition during the impact does not happen in the entire volume of the NP at once, but during each impact only a part of the NP melts. We, however, note here that polycrystallinity may result from fast quenching after the impact of the entirely molten NP, as was shown in [3].

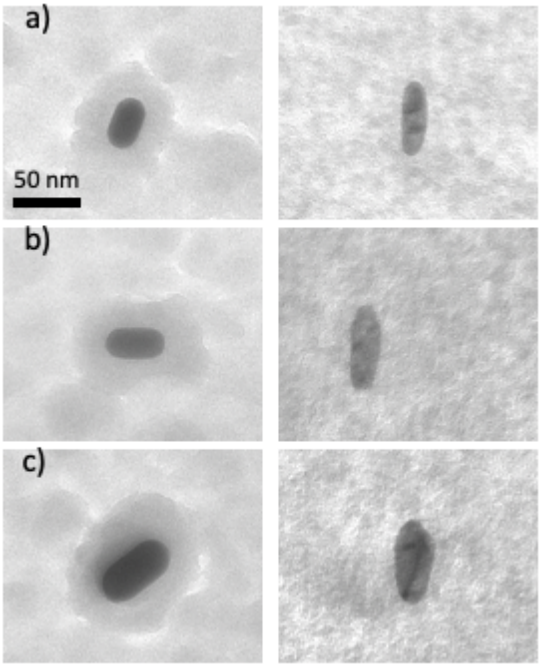


FIG. 3. TEM images of single nanorods sandwiched between two 50 nm PECVD $SiO_2$ layers with different initial size that "rotate" after the irradiation with $^{127}I$ at $10^{14}$ ions/cm$^2$.(a) Length=34.3 nm and diameter=21.2 nm),(b)length=38.5 nm and diameter=20.3 nm and (c) length=53 nm and diameter=32 nm (the left image is before and the right is after the irradiation).

To understand the rotation mechanism of the irradiated nanorods, we performed a series of simulations using

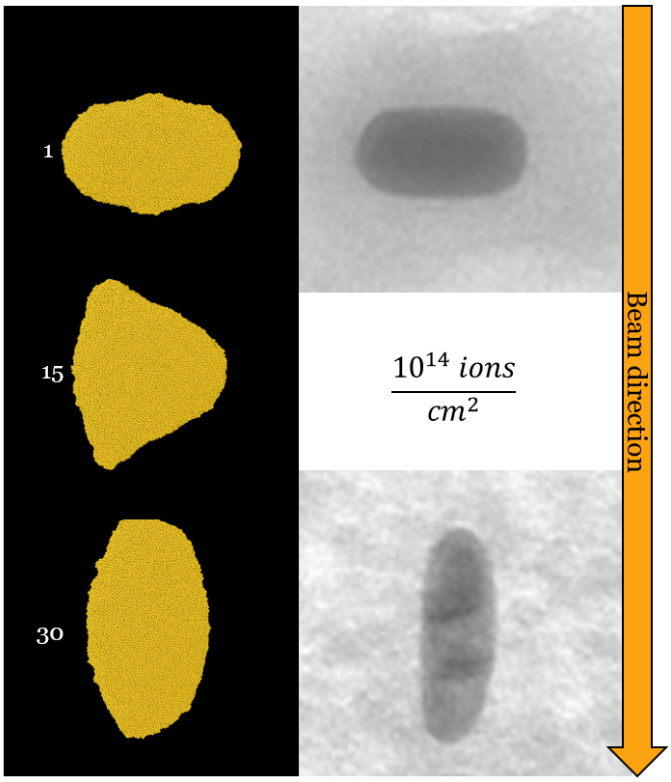


FIG. 4. Left: Nanoparticle shape after simulating 1, 15, and 30 impacts to random positions on the nanorod with 164 MeV $^{197}$Au ion. Right: Zoom in of the same nanorod as in Fig. 3 b).

the deposited energy profiles corresponding to 50 MeV $^{197}$I and 164 MeV $^{197}$Au ions. In these simulations, we saw that the first ion impacts induced formation of surface protrusions grown from the nanorods at the impact locations (see e.g. the top left image in figure 4). Both deposited energy profiles gave similar results. Consecutive impacts add more localized protrusions, which gradually accumulate and cause shape transformation of the entire nanorod into at first, a spheroidal and then an elongated shape of a nanorod.

Since the dynamics of these modifications is faster under the impacts of higher energy, we show in the left panel of figure 4 the evolution of shape modification of the nanorod irradiated by 164 MeV $^{197}$Au. For comparison, similar images of the experimental nanorod are shown in the right panel. We follow the shape evolution by adding the ion tracks subsequently at random locations of the nanorod perpendicular to its major axis. Already after the first 15 impacts, the shape had incrementally changed to an asymmetrical spheroid, see the middle image in the left panel of figure 4, where the spheroid with a more elongated left side is shown. After the next 15 impacts, the shape is fully transformed into a rod in the beam direction, see the lowest image in the left panel of figure 4 and the corresponding experimental image on the lowest right. Although dimensions are different, the changes are proportional, with similar elongation observed after irradiation in both simulation and experiment.

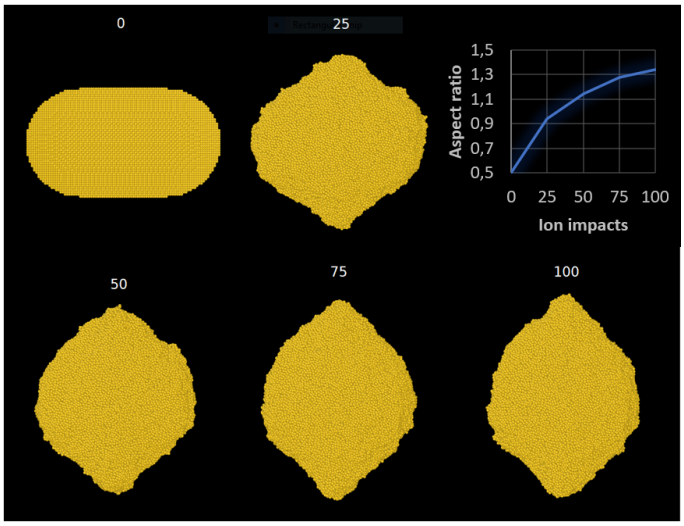


FIG. 5. Nanorod shape after 0, 25, 50, 75, and 100 simulated 50 MeV $^{127}$I ion impacts to the center of the nanorod.

The simulations of ion impacts of 50 MeV $^{127}$I on the same size of the nanorod are shown in figure 5. We see that under this energy, the shape of the nanorod changes much slower due to lower energy deposition. The results, however, are similar to those obtained for the 164 MeV $^{197}$Au ions, i.e. small incremental changes transformed the nanorod oriented perpendicular to the beam into the nanorod oriented in the beam direction. Thus we conclude that although the nanorod changes visibly its orientation, the change does not require the actual rotation within the solid matrix. The modification is guided by the dynamics of density changes in the matrix and material flow due to relaxing of overpressured liquid phase of nanorods during the impact and fast quenching after it, as previously described for initially spherical systems [3]. The small incremental changes accumulate and result in growth in the beam direction, and loss of length in others. This finally leads to a nanorod aligning in the beam direction.

We still consider why the largest nanorods, such as the one marked with a blue arrow in Fig. 2, are not rotated. Previously, Rizza et al. [37] studied the size dependence of spherical nanoparticles on melting and concluded that large particles do not melt and are not deformed noticeably. In the recent study, we extended this model to nanorods including different possible interface effects on heat dynamics during the impact on a nanorod [38]. In these simulations we saw that the energy deposited by a SHI in the large nanorods (40nm×80nm) is not sufficient for melting even if all resistive effects for heat flow through the interface are taken into account[38]. Hence, no shape modification, including rotation, can be

expected for very large nanorods.

In conclusion, using both experiments and simulations, we show how swift heavy ions with energies readily available in typical tandem accelerators can be used to rotate nanorods, which are embedded in a solid amorphous matrix. In the experiments, we used TEM windows to track changes in individual nanorods. We observed that nanorods laid in a plane with a 45° angle to the beam direction rotated to align with the beam. By using a multiscale simulation model of the effect of electronic excitations on atom dynamics, we explain the change of nanorod orientation by an overpressure mechanism, and show that the apparent rotation is a result of small incremental shape modifications rather than an actual rotation of the nanorod as a whole. Our results show that swift heavy ions even of relatively low energies can be used as a means to control the orientation of metal nanorods buried inside a protective insulating material.

*Acknowledgements.* We gratefully acknowledge the Academy of Finland NANOIS project (project number 309730) for financial support. V. Jantunen, A. Leino, and F. Djurabekova gratefully acknowledge IT Centre of Science CSC in Espoo, Finland for providing CPU resource grants.

[1] S. Link and M. A. El-Sayed, Spectral properties and relaxation dynamics of surface plasmon electronic oscillations in gold and silver nanodots and nanorods, The Journal of Physical Chemistry B **103**, 8410 (1999).

[2] A. A. Leino, O. H. Pakarinen, F. Djurabekova, and K. Nordlund, A study on the elongation of embedded au nanoclusters in sio2 by swift heavy ion irradiation using md simulations, Nuclear Instruments and Methods in Physics Research Section B: Beam Interactions with Materials and Atoms **282**, 76 (2012).

[3] A. A. Leino, O. Pakarinen, F. Djurabekova, K. Nordlund, P. Kluth, and M. C. Ridgway, Swift heavy ion shape transformation of au nanocrystals mediated by molten material flow and recrystallization, Materials Research Letters **2**, 37 (2014).

[4] E. Dawi, A. Vredenberg, G. Rizza, and M. Toulemonde, Ion-induced elongation of gold nanoparticles in silica by irradiation with ag and cu swift heavy ions: track radius and energy loss threshold, Nanotechnology **22**, 215607 (2011).

[5] O. Peña-Rodríguez, A. Prada, J. Olivares, A. Oliver, L. Rodríguez-Fernández, H. G. Silva-Pereyra, E. Bringa, J. M. Perlado, and A. Rivera, Understanding the ion-induced elongation of silver nanoparticles embedded in silica, Scientific Reports **7**, 1 (2017).

[6] C. D'orleans, J. Stoquert, C. Estournes, J. Grob, D. Muller, J. Guille, M. Richard-Plouet, C. Cerruti, and F. Haas, Elongated co nanoparticles induced by swift heavy ion irradiations, Nuclear Instruments and Methods in Physics Research Section B: Beam Interactions with Materials and Atoms **216**, 372 (2004).

[7] S. Klaumünzer, Modification of nanostructures by high-energy ion beams, Nuclear Instruments and Methods in Physics Research Section B: Beam Interactions with Materials and Atoms **244**, 1 (2006).

[8] K. Awazu, X. Wang, M. Fujimaki, J. Tominaga, H. Aiba, Y. Ohki, and T. Komatsubara, Elongation of gold nanoparticles in silica glass by irradiation with swift heavy ions, Physical Review B **78**, 054102 (2008).

[9] K. Awazu, X. Wang, T. Komatsubara, J. Watanabe, Y. Matsumoto, S. Warisawa, and S. Ishihara, The fabrication of aligned pairs of gold nanorods in sio2 films by ion irradiation, Nanotechnology **20**, 325303 (2009).

[10] E. Dawi, G. Rizza, M. Mink, A. Vredenberg, and F. Habraken, Ion beam shaping of au nanoparticles in silica: Particle size and concentration dependence, Journal of Applied Physics **105**, 074305 (2009).

[11] P. Kluth, R. Giulian, D. Sprouster, C. Schnohr, A. Byrne, D. Cookson, and M. Ridgway, Energy dependent saturation width of swift heavy ion shaped embedded au nanoparticles, Applied Physics Letters **94**, 113107 (2009).

[12] D. Avasthi, Y. Mishra, F. Singh, and J. Stoquert, Ion tracks in silica for engineering the embedded nanoparticles, Nuclear Instruments and Methods in Physics Research Section B: Beam Interactions with Materials and Atoms **268**, 3027 (2010).

[13] M. C. Ridgway, R. Giulian, D. J. Sprouster, P. Kluth, L. L. Araújo, D. Llewellyn, A. Byrne, F. Kremer, P. F. P. Fichtner, G. Rizza, *et al.*, Role of thermodynamics in the shape transformation of embedded metal nanoparticles induced by swift heavy-ion irradiation, Physical review letters **106**, 095505 (2011).

[14] H. Amekura, N. Ishikawa, N. Okubo, M. C. Ridgway, R. Giulian, K. Mitsuishi, Y. Nakayama, C. Buchal, S. Mantl, and N. Kishimoto, Zn nanoparticles irradiated with swift heavy ions at low fluences: Optically-detected shape elongation induced by nonoverlapping ion tracks, Physical Review B **83**, 205401 (2011).

[15] Y. Mishra, F. Singh, D. Avasthi, J. Pivin, D. Malinovska, and E. Pippel, Synthesis of elongated au nanoparticles in silica matrix by ion irradiation, Applied Physics Letters **91**, 063103 (2007).

[16] H. Amekura, P. Kluth, P. Mota-Santiago, I. Sahlberg, V. Jantunen, A. A. Leino, H. Vázquez, K. Nordlund, F. Djurabekova, N. Okubo, *et al.*, Vaporlike phase of amorphous si o 2 is not a prerequisite for the core/shell ion tracks or ion shaping, Physical Review Materials **2**, 096001 (2018).

[17] C. d'Orléans, J. Stoquert, C. Estournes, C. Cerruti, J. Grob, J. Guille, F. Haas, D. Muller, and M. Richard-Plouet, Anisotropy of co nanoparticles induced by swift heavy ions, Physical Review B **67**, 220101 (2003).

[18] C. d'Orléans, J. Stoquert, C. Estournes, C. Cerruti, J. Grob, J. Guille, F. Haas, D. Muller, and M. Richard-Plouet, Anisotropy of Co nanoparticles induced by swift heavy ions, Physical Review B **67**, 220101 (2003).

[19] S. Roorda, T. van Dillen, A. Polman, C. Graf, A. van Blaaderen, and B. J. Kooi, Aligned gold nanorods in silica made by ion irradiation of core–shell colloidal particles, Advanced Materials **16**, 235 (2004).

[20] M. Toulemonde, W. Assmann, C. Dufour, A. Meftah, F. Studer, and C. Trautmann, Experimental phenomena and thermal spike model description of ion tracks in amorphisable inorganic insulators, Mat. Fys. Medd **52**, 263 (2006).

[21] I. Lifshits, M. Kaganov, and L. Tanatarov, On the theory of radiation-induced changes in metals, Journal of Nuclear Energy. Part A. Reactor Science **12**, 69 (1960).

[22] S. Anisimov, B. Kapeliovich, T. Perelman, *et al.*, Electron emission from metal surfaces exposed to ultrashort laser pulses, Zh. Eksp. Teor. Fiz **66**, 375 (1974).

[23] A. Leino, S. Daraszewicz, O. H. Pakarinen, K. Nordlund, and F. Djurabekova, Atomistic two-temperature modelling of ion track formation in silicon dioxide, EPL (Europhysics Letters) **110**, 16004 (2015).

[24] M. Laitinen, M. Rossi, J. Julin, and T. Sajavaara, Time-of-flight – energy spectrometer for elemental depth profiling – jyväskylä design, Nuclear Instruments and Methods in Physics Research Section B: Beam Interactions with Materials and Atoms **337**, 55 (2014).

[25] PARCAS Computer code 1996-2021, available open source at https://gitlab.com/acclab/parcas/. The main principles of the molecular dynamics algorithms are presented in [39, 40]. The adaptive time step and electronic stopping algorithms are the same as in [41]. The 2016 version of the code is published in the supplementary material to Ref. [42].

[26] F. Djurabekova and K. Nordlund, Atomistic simulation of the interface structure of si nanocrystals embedded in amorphous silica, Physical Review B **77**, 115325 (2008).

[27] M. Toulemonde, W. Assmann, C. Dufour, A. Meftah, F. Studer, and C. Trautmann, Experimental phenomena and thermal spike model description of ion tracks in amorphisable inorganic insulators, Mat. Fys. Medd **52**, 263 (2006).

[28] T. Watanabe, D. Yamasaki, K. Tatsumura, and I. Ohdomari, Improved interatomic potential for stressed si, o mixed systems, Applied surface science **234**, 207 (2004).

[29] J. Samela, K. Nordlund, V. N. Popok, and E. E. Campbell, Origin of complex impact craters on native oxide coated silicon surfaces, Physical Review B **77**, 075309 (2008).

[30] S. Foiles, M. Baskes, and M. S. Daw, Embedded-atom-method functions for the fcc metals cu, ag, au, ni, pd, pt, and their alloys, Physical Review B **33**, 7983 (1986).

[31] S. Foiles, M. Baskes, and M. Daw, Erratum: Embedded-atom-method functions for the fcc metals cu, ag, au, ni, pd, pt, and their alloys, Physical Review B **37**, 10378 (1988).

[32] J. F. Ziegler and J. P. Biersack, The stopping and range of ions in matter, in *Treatise on heavy-ion science* (Springer, 1985) pp. 93–129.

[33] H. J. Berendsen, J. v. Postma, W. F. van Gunsteren, A. DiNola, and J. R. Haak, Molecular dynamics with coupling to an external bath, The Journal of chemical physics **81**, 3684 (1984).

[34] P. Mota-Santiago, F. Kremer, A. Nadzri, M. C. Ridgway, and P. Kluth, Elongation of metallic nanoparticles at the interface of silicon dioxide and silicon nitride, Nuclear Instruments and Methods in Physics Research Section B: Beam Interactions with Materials and Atoms **409**, 328 (2017).

[35] F. Corni, A. Monelli, G. Ottaviani, R. Tonini, G. Queirolo, and L. Zanotti, Radiation enhanced transport of hydrogen in sio2, Journal of non-crystalline solids **216**, 71 (1997).

[36] G. Rizza, E. Dawi, A. Vredenberg, and I. Monnet, Ion engineering of embedded nanostructures: From spherical to facetted nanoparticles, Applied Physics Letters **95**, 043105 (2009).

[37] G. Rizza, P. Coulon, V. Khomenkov, C. Dufour, I. Monnet, M. Toulemonde, S. Perruchas, T. Gacoin, D. Mailly, X. Lafosse, *et al.*, Rational description of the ion-beam shaping mechanism, Physical Review B **86**, 035450 (2012).

[38] V. Jantunen, A. L. M. Veske, A. Kyritsakis, H. V. Muiños, K. Nordlund, and F. Djurabekova, Journal of Physics D: Applied Physics (submitted).

[39] K. Nordlund, M. Ghaly, R. Averback, M. Caturla, T. D. de La Rubia, and J. Tarus, Defect production in collision cascades in elemental semiconductors and fcc metals, Physical Review B **57**, 7556 (1998).

[40] M. Ghaly, K. Nordlund, and R. S. Averback, Molecular dynamics investigations of surface damage produced by kiloelectronvolt self-bombardment of solids, Philosophical Magazine A **79**, 795 (1999).

[41] K. Nordlund, Molecular dynamics simulation of ion ranges in the 1–100 kev energy range, Computational materials science **3**, 448 (1995).

[42] F. Granberg, K. Nordlund, M. W. Ullah, K. Jin, C. Lu, H. Bei, L. Wang, F. Djurabekova, W. Weber, and Y. Zhang, Mechanism of radiation damage reduction in equiatomic multicomponent single phase alloys, Physical review letters **116**, 135504 (2016).